ACS APPLIED MATERIALS & INTERFACES

Research Article

www.acsami.org

Polymer Nanowrinkles with Continuously Tunable Wavelengths

Mark D. Huntington,[†] Clifford J. Engel,[‡] Alexander J. Hryn,[†] and Teri W. Odom*[,†,‡]

[‡]Department of Chemistry and [†]Department of Materials Science and Engineering, Northwestern University, Evanston, Illinois 60208, United States

Supporting Information

ABSTRACT: This paper describes a parallel method to generate polymer nanowrinkles over large areas with wavelengths that were continuously tuned down to 30 nm. Reactive ion etching using fluorinated gases was used to chemically treat thermoplastic polystyrene films, which resulted in a stiff skin layer. Upon heating, the treated thermoplastic, microscale, and nanoscale wrinkles were formed. We used variable-angle spectroscopic ellipsometry to characterize the thickness of the skin layer; this thickness could then be used to predict and control the nanowrinkle wavelength. Because the properties of these nanotextured polymer surfaces can be tuned over a large range of wrinkle wavelengths, they are promising for a broad range of applications, especially those that require large-area and uniform surface patterning.

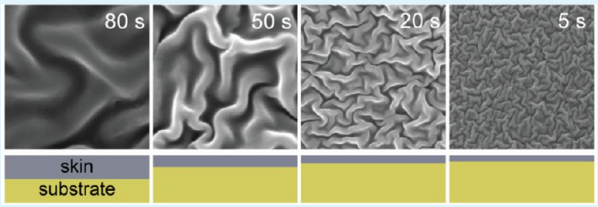

KEYWORDS: *nanowrinkles, polymers, nanotexturing, polystyrene, reactive ion etching*

INTRODUCTION

Nanotextured surfaces in natural and fabricated systems can change the optical or mechanical properties of a surface without affecting the bulk properties of the material.[1−4] One method to create texturing is to buckle a stiff skin layer on a softer, prestrained substrate by allowing the substrate to relax, which compresses the skin layer. The substrate is typically prestrained by thermal[5,6] or mechanical[1,7−9] expansion. The resulting wrinkles are characterized by wavelength $\lambda = 2\pi h_S(E_S/E_B)^{1/3}$, where h_S is the thickness of the skin layer, E_S is Young's modulus of the skin, and E_B is Young's modulus of the substrate.[1,8,10] The wrinkle amplitude (A) is proportional to λ and the applied strain (ε) from the substrate.[1,5,8,10] Because wrinkling is a general phenomenon, wrinkle wavelengths can span several orders of magnitude, from 10^4 to 10^{-8} m.[2,8]

Wrinkling of the skin layer has emerged as a simple method to fabricate microscale[5,7] and nanoscale surface textures.[4,8,11−13] The periodicity and amplitude of buckling can be engineered through the applied strain and material properties of the skin and substrate. There are two general approaches to create skin layers on elastomeric substrates. One method is to deposit a thin layer of material on a prestrained substrate whose Young's modulus is less than that of the deposited layer.[5,7] Another method is to modify the top layer of a prestrained substrate with a plasma,[7,14−16] ion beam,[3,17] or ultraviolet light[6,18] to increase the modulus of the skin layer. For the former method, the skin thickness of a deposited layer can be easily controlled. For a gold layer on a polystyrene (PS) thermoplastic substrate, the minimum thickness to have a continuous layer is ∼5 nm, which puts a lower limit on the wrinkle wavelength of ∼200 nm.[7] One way to achieve wrinkle wavelengths below 200 nm is to reduce the modulus of the skin layer. For example, O_2 plasma treatment of mechanically stretched poly(dimethylsiloxane) (PDMS), which forms a silica skin,[1,9,16,19,20] can result in wrinkles as small as 50 nm.[1,16] Because the optical properties of the skin and substrate were similar, however, the skin thickness was difficult to measure directly,[20] which limited control of the resulting wrinkle wavelengths.

Recently, micro- and nanowrinkled structures have been used in optical and electronic devices to increase their efficiency and stability under mechanical deformations.[4,11,13,21] How this surface texturing enhances the properties of these devices, however, remains largely unknown. To design devices that take advantage of these surface textures, new material systems (skin and substrate materials) need to be developed. Furthermore, to understand the mechanisms that result in these improvements, a strategy to vary the wrinkle wavelength systematically in the nanometer regime is needed. Critically, a method to measure the skin thickness accurately, which can be used to determine the ratio of Young's moduli of the skin and substrate, is required to predict and control the wrinkle wavelength at the nanometer scale.

Here we describe a chemical patterning method based on reactive ion etching (RIE) that can generate polymer nanowrinkles with tunable wavelengths. We found that the skin depth and wrinkle wavelength could be controlled by changing either (i) the gas used in the RIE treatment or (ii) the plasma exposure time for a specific RIE plasma gas. We fabricated wrinkles with λ ranging from 250 to 50 nm by chemically treating PS thermoplastic films with RIE gases SF_6, CF_4, CHF_3, or Ar. Unique to the CHF_3 gas, the wrinkle wavelength could be tuned from several micrometers to as small as 30 nm simply by decreasing the RIE exposure time. To

Received: June 4, 2013
Accepted: June 12, 2013
Published: June 12, 2013

   dx.doi.org/10.1021/am402166d | ACS Appl. Mater. Interfaces 2013, 5, 6438−6442

determine how these chemical treatments resulted in wavelength-tunable nanowrinkles, we developed a method to measure the skin layer thickness using variable-angle spectroscopic ellipsometry (VASE).

RESULTS AND DISCUSSION

Figure 1 depicts how nanowrinkles with different wrinkle wavelengths can be generated over large-area (>100 cm^2)

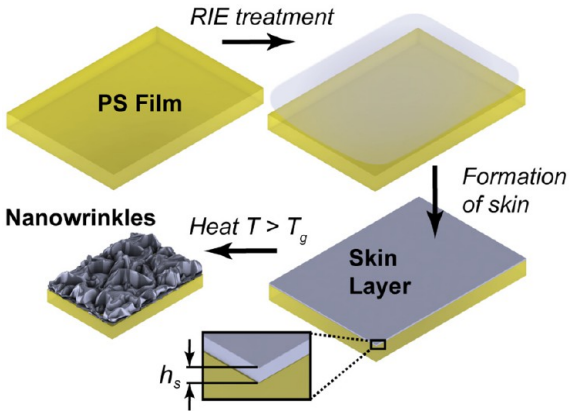

Figure 1. Nanowrinkled surfaces made from a PS thermoplastic sheet. Starting with a commercially available thermoplastic sheet, we exposed one side to an RIE plasma. The RIE treatment caused a thin skin layer to form on a PS substrate. The thickness of the skin (h_S) was measured using VASE. The treated PS was shrunk (ε = 0.5) in an oven at T = 125 °C.

substrates. First, as-bought PS films were plasma-treated in a RIE system with plasma gases of Ar, SF_6, CF_4, or CHF_3 and exposure times from 5 to 80 s (see the Methods section). RIE treatment of the PS films created a skin layer with a refractive index (n) different from that of the bulk PS; hence, the thickness of this skin layer (h_S) could be measured with ellipsometry. The chemically treated PS was then heated above its glass transition temperature (T_g = 100 °C) until the strain applied to the skin layer was ε = 0.5.

Figure 2 shows scanning electron microscopy (SEM) images of nanowrinkles, with different wrinkle wavelengths, produced by exposing PS to the four different RIE plasmas (SF_6, CF_4, CHF_3, and Ar). Because of the limited penetration depth of plasma gases into PS substrates,[22,23] we expected that E_B would remain constant while E_S and h_S would vary depending on the type of gas used. Previous X-ray photoelectron spectroscopy (XPS) studies on the chemical structure of PS films after RIE treatment have shown that Ar bombardment caused cross-linking in the top layer of the PS substrate, while SF_6, CF_4, and CHF_3 bombardment fluorinated the carbon backbone in the top several nanometers of the film.[22,23] Both of these processes created a stiff skin layer on top of the PS substrate. To ensure that the differences in the wrinkle wavelength were attributed to the different gases, we kept the flow rate, power, pressure, and time (30 s) constant during the RIE process. SF_6 and CF_4 gases generated nanowrinkles with $\lambda \approx 50$ nm (Figure 2a,b), and CHF_3 gas produced wavelengths of ~160 nm (Figure 2c). Ar plasma produced the largest wrinkles with $\lambda \approx 250$ nm (Figure 2d). For all samples, the average wavelength was determined from the 2D fast Fourier transform (FFT) of SEM images (Supporting Information, Figures S1 and S2). Because the nanowrinkle orientation was randomly distributed, the 2D FFT

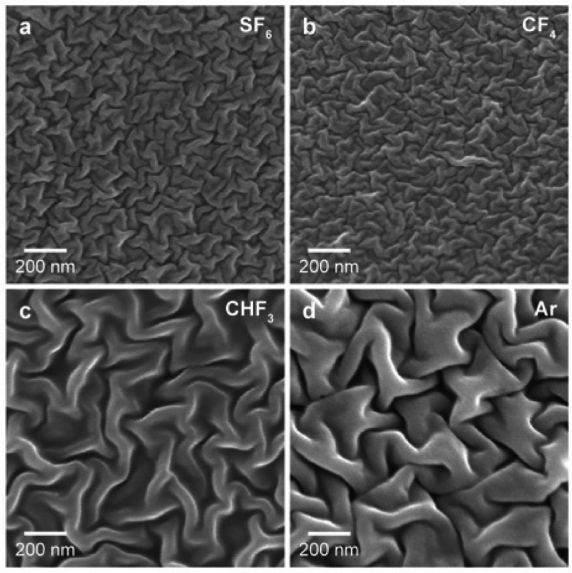

Figure 2. Chemical modification of PS films resulting in nanowrinkles with different wavelengths. SEM images of 2D nanowrinkles formed by RIE with (a) SF_6 (λ = 50 nm), (b) CF_4 (λ = 50 nm), (c) CHF_3 (λ = 160 nm), and (d) Ar (λ = 250 nm). All other RIE parameters including the radio-frequency power, chamber pressure, gas flow rate, and treatment time were held constant.

showed a ring of high intensity about the center of the transform. To find the wrinkle wavelength, we took a radial average of the 2D FFT and found the peak of that average (Supporting Information).

The wavelengths of wrinkles prepared with SF_6, CF_4, and Ar plasma exposures were invariant even when the treatment time, power, pressure, or flow rate were varied independently (up to ±50%). In contrast, wrinkles formed after CHF_3 treatment could be continuously tuned from 30 to 500 nm by increasing the plasma exposure time from 5 to 80 s (Figure 3). Larger microwrinkles (λ >500 nm) could also be made with longer exposure times; here, however, we focus on the wrinkles in the nanometer and submicrometer regimes. Figure S3 in the Supporting Information shows a plot of the different wavelengths that resulted by varying the exposure time with CHF_3. We found that λ increased approximately linearly (R^2 = 0.99) with exposure times over the range 5−80 s with a slope of 5.2 nm/s. We used this slope to calibrate the RIE time to make samples at specific wrinkle wavelengths. RIE has control over exposure times within ±1 s; therefore, the average wrinkle wavelength could be controlled to ±5 nm. To verify this control, we acquired six wavelength measurements for each RIE exposure time. Measurement variations in the wrinkle wavelength are indicated by error bars in Figure S3 in the Supporting Information. The change in the wrinkle wavelength can be attributed to changes in h_S and/or E_S. In order to determine which of these parameters is the main contributing factor, the thickness of the skin layer must be measured.

There are several methods for characterizing the thickness of a thin polymer layer. Alternating between secondary-ion mass spectrometry (SIMS) or XPS and dry etching can be used to determine the thickness of transparent films on transparent substrates, such as skin layers made by the RIE treatment of PS films.[22,24,25] Together, these techniques are destructive. When we used SIMS to characterize the substrates, charging at the sample surface caused the fluorine molecules to reattach to the

dx.doi.org/10.1021/am402166d | ACS Appl. Mater. Interfaces 2013, 5, 6438−6442

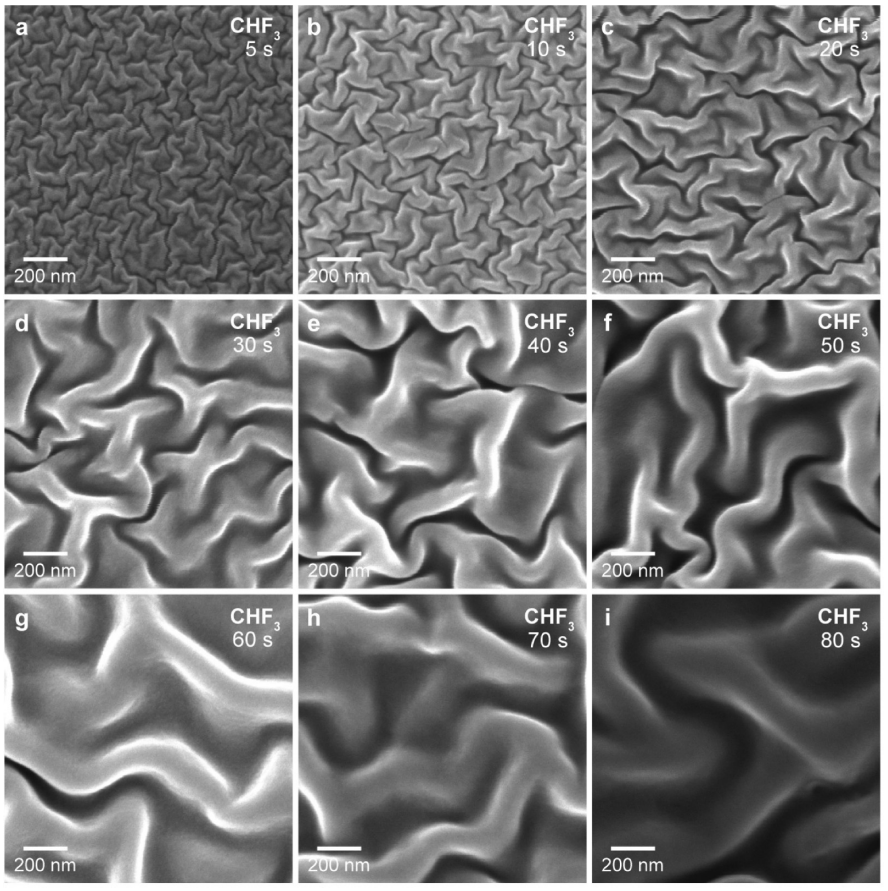

Figure 3. Characteristic wavelengths of PS films tuned by changing the RIE exposure time. SEM images of 2D nanowrinkles formed by RIE with CHF_3 and times of (a) 5 s (λ = 34 nm), (b) 10 s (λ = 44 nm), (c) 20 s (λ = 107 nm), (d) 30 s (λ = 162 nm), (e) 40 s (λ = 198 nm), (f) 50 s (λ = 228 nm), (g) 60 s (λ = 303 nm), (h) 70 s (λ = 360 nm), and (i) 80 s (λ = 431 nm).

surface of the PS, which prevented accurate measurements of the thickness of the skin layer. Therefore, we took advantage of a change in the refractive index of the skin layer caused by RIE treatment. VASE is a nondestructive technique that is typically used to determine the optical properties of both thin films and bulk materials as well as film thicknesses.[26,27] Combining spectroscopic measurements over multiple angles of incidence allows for the simultaneous determination of the layer thickness and optical constants.[26] VASE also has the flexibility to characterize structures that single-angle and/or single-wavelength ellipsometry cannot. For example, VASE can be used to measure multilayer films with unknown optical properties;[26] thus, we used this method to measure the skin layers on the RIE-treated PS films.

Figure 4a shows a scheme of an ellipsometry measurement of the skin layer on a PS substrate. VASE detects changes in the polarization of light, expressed by the ellipsometry constants Ψ and Δ reflected off or transmitted through a sample surface at different incident angles (φ) over a range of wavelengths. The optical properties of thin film layers, as well as those of the substrate, can be determined simultaneously by fitting Ψ and Δ across multiple wavelengths to the architecture of the sample (e.g., PS substrate/skin layer/air).[26,27] Because PS is transparent at optical frequencies, we used a three-parameter Cauchy model ($A + B\lambda^{-2} + C\lambda^{-4}$)[26] to fit Ψ and Δ over the measurement range (380−1000 nm) for both the substrate and skin layer. Reflection measurements were taken at six different incident angles near Brewster's angle for PS (φ_B = 57.9°), which increased the sensitivity of our measurement of both the skin thickness and optical properties (see the Methods section). To increase the accuracy of skin thickness measurements, we kept the refractive index and thickness of the substrate constant throughout our measurements, and only fit the refractive index and thickness of the skin layer. Because the fabrication of bulk PS does not always produce the same PS structure, the refractive index of our PS substrate can vary from the literature values (n_{lit} = 1.587 at λ = 0.6238 μm).[28] Therefore, we first characterized the refractive index of the substrate (n_{meas} = 1.571 at λ = 0.6238 μm) by measuring the transmission and reflection from an untreated PS film and used these values for all subsequent experiments. We also roughened the (untreated) back of all of the samples to eliminate artifacts due to reflections from the back surface of the PS film. Roughening did not affect the wrinkle properties on the top of the sample.

Table 1 summarizes n and the Cauchy coefficients of the skin layers formed after the different chemical treatments. As expected, n decreased for substrates treated with a fluorine-rich plasma compared to bulk PS because fluoropolymers typically have a refractive index ($n \approx 1.3$)[28] lower than PS ($n \approx 1.5$).[28] In contrast, n of Ar-treated samples increased slightly ($\Delta n \approx 0.02$); this increase is likely from a higher density of polymer in the skin layer, which is a result of the increased cross-linking induced by the Ar treatment.[23] For the CHF_3-treated PS substrate, we calculated n = 1.379 (at 0.6238 μm) of the skin layer using the same parameters as the bulk PS measurements.

dx.doi.org/10.1021/am402166d | ACS Appl. Mater. Interfaces 2013, 5, 6438−6442

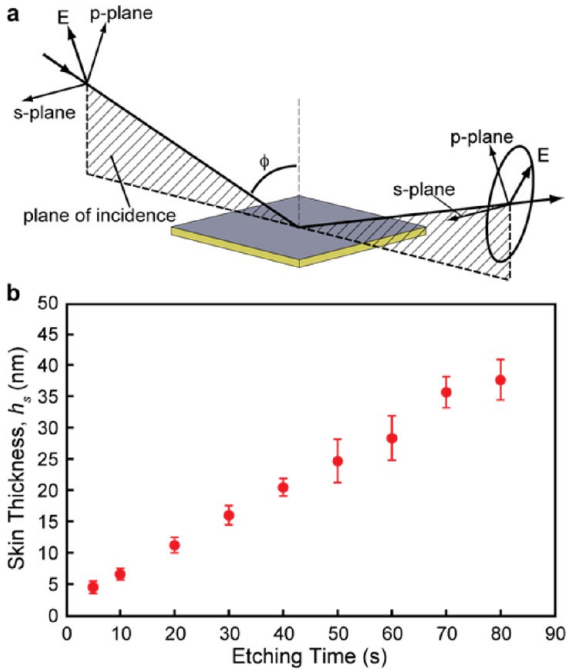

Figure 4. Skin layer thickness measured by ellipsometry. (a) Diagram of how light interacts with the surface of the RIE-treated PS sample.[26] (b) Skin thickness measurements at nine different treatment times for CHF_3-treated PS films. Each data point represents 24 independent measurements.

Table 1. Refractive Index Data and Cauchy Coefficients (380−1000 nm) of the Different Skin Layers [SF_6 (t = 30 s), CF_4 (t = 30 s), CHF_3 (t = 80 s), and Ar (t = 30 s)] Measured via VASE

gas type	n (0.6328 μm)	h_S (nm)	A	B (μm^2)	C (μm^4)
None	1.571	N/A	1.55	7.3×10^{-3}	4.3×10^{-4}
CHF_3	1.379	38	1.37	2.2×10^{-3}	6.6×10^{-4}
CF_4	1.445	5	1.29	9.0×10^{-2}	-1.2×10^{-2}
SF_6	1.465	7	1.39	3.7×10^{-2}	-4.2×10^{-3}
Ar	1.595	23	1.57	2.1×10^{-3}	1.9×10^{-3}

In addition to measuring the optical properties, we used VASE to determine the thickness of the CHF_3 layer at different RIE treatment times. We found that the Cauchy coefficients (and refractive indices) of the CHF_3-treated substrates did not change significantly with exposure time. Therefore, we used the parameters obtained from the sample with the thickest skin layer (t = 80 s) to measure h_S for all of the CHF_3-treated samples because this layer gave the most accurate measurement of the optical properties. We characterized four samples in separate RIE processes; on each sample, measurements were taken at six different locations. Figure 4b shows how the thickness of the CHF_3 skin layer increased with longer RIE exposure times; error bars represent the standard deviation across the 24 measurements. We found that variation in the skin thickness mostly depended on the spatial location of the sample inside the RIE chamber. Therefore, most of the deviation was a result of a lack of spatial uniformity of the plasma rather than uncertainty in the VASE measurement. Because the thicknesses of the CF_4 and SF_6 layers did not change with variations in the RIE conditions, the accuracy of the thickness measurement can be estimated to ±1 nm.

Figure 5 shows the relationship between the skin thickness and wrinkle wavelength for all RIE gases tested at ε = 0.5.

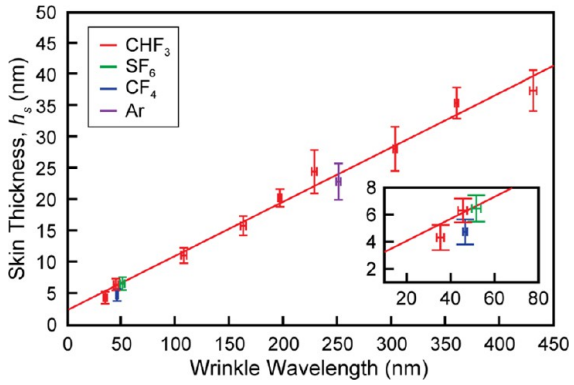

Figure 5. Wrinkle wavelength increasing linearly with the skin thickness. The linear fit is for the CHF_3 values only and gives an R^2 value of 0.985 and a slope corresponding to E_S/E_B = 6.2. The ratios of the skin thickness to the wrinkle wavelength for CF_4, SF_6, and Ar are close to the trend line for CHF_3, indicating a similar E_S/E_B ratio.

Because we consider plasma-treated samples as two discrete layers, skin and substrate, the wrinkle wavelength is directly proportional to the thickness of the skin.[1,5] We found a linear relationship (R^2 = 0.985) between the wrinkle wavelength and skin thickness (Figure 5), which suggests that only h_S is changing while the ratio E_S/E_B remained constant with increased RIE exposure times. One explanation for the increase in h_S is that, at longer treatment times, the penetration depth of the CHF_3 gas increased. From the slope of the line-of-best-fit, we extracted that E_S/E_B = 6.2, which is ∼10 times smaller than the previously reported ratios for silica on PDMS[1,5,7,8] and ∼5 times smaller for gold on PS.[7] A smaller E_S/E_B ratio enables access to smaller wrinkle wavelengths compared to other systems with the same skin thickness. For example, we could achieve 50-nm wrinkle wavelengths with a 5-nm skin thickness; however, with the same thickness of gold on PS, 200-nm wrinkles were formed.[7]

For PS substrates treated with SF_6, CF_4, and Ar, we also determined the skin thickness based on refractive index differences between the skin and substrate. The thickness of the CF_4-treated skin layer ($h_S \approx 5$ nm) was similar to that of the SF_6 layer ($h_S \approx 7$ nm), while the Ar-treated layer was thicker ($h_S \approx 23$ nm; Figure 5). The thickness of the skin layer for the CHF_3 sample ($h_S \approx 16$ nm) treated for 30 s fell between the values for SF_6- and Ar-treated samples. We found the thickness of the SF_6 layer to be ca. 7, which matches well with the previously measured values of 3−9 nm found using XPS on a PS film treated with SF_6.[23] Because the thicknesses of the skin layers produced by Ar, CF_4, and SF_6 treatment do not vary with changes in the RIE conditions, it was not possible to plot a trend line similar to the line for CHF_3 for these treatments. However, when plotted against their wavelengths, the skin thickness values for the other gas treatments (Ar, CF_4, and SF_6) fell close to the trend for CHF_3 (Figure 5), which indicates that the ratio E_S/E_B for these systems is similar to that for the skin layers and substrates made by treating PS with CHF_3 plasma.

CONCLUSION

In summary, we presented a massively parallel method to create nanometer-scale textures with unprecedented control over the

wrinkle periodicity. Our nanotexturing process relies on a chemical patterning method that can form sub-30-nm polymer wrinkles over large (>200 cm^2) areas starting from store-bought PS substrates. By varying the exposure times of RIE treatments, we could tune the wrinkle wavelength from 30 to 500 nm; thus, it is now possible to fabricate substrates with specific wrinkle wavelengths with ±5 nm accuracy in average wavelength. Additionally, we showed that VASE could be used to characterize skin thicknesses down to 5 nm with refractive index differences as small as 0.02. We anticipate that the characterization and tunability of our nanowrinkle system will facilitate the use of nanowrinkles in optical and electronic applications such as high-efficiency organic solar cells or as surface-plasmon-enhanced Raman spectroscopy substrates.

METHODS

Fabrication of 2D Nanowrinkles. 2D nanowrinkled surfaces on PS films were created by the following methods: (i) cleaning as-bought PS films (Grafix shrink film) with isopropyl alcohol and distilled water; (ii) treating the PS films with a plasma in a RIE system (Samco RIE-10NR) for 5−80 s with the following conditions: gases Ar, SF_6, CF_4, or CHF_3, flow rate of 20 sccm, power of 70 W, and pressure at 20 Pa; (iii) heating the chemically treated PS in a convection oven at 125 °C until the films shrunk to ε = 0.5. 2D nanowrinkle surfaces were then coated with ∼8 nm of AuPd for SEM imaging.

Ellipsometry Measurements of the Skin Thickness. The thicknesses of the skin layers were determined using an M-2000U variable-angle spectroscopic ellipsometer (J. A. Woollam Co.) over a wavelength range of 380−1000 nm and over incident angles from 55 to 60° in 1° increments. First, the transmission and reflection of an untreated, bulk PS substrate was measured, and its refractive index values were held constant in the skin−substrate model for all subsequent experiments. Then, reflection of the RIE-treated PS substrates was measured over the same angles and wavelength range. The back sides of all samples, including the reference, were roughened using 1000 grit waterproof sandpaper (Norton) to avoid artifacts because of reflections from the back surface of the PS film. For each gas and etching time, four samples were made in independent RIE processes. Each data point was based on six measurements from different locations on these four samples.

ASSOCIATED CONTENT

Supporting Information

Integration of the 2D FFT, determination of 2D wrinkle wavelengths using FFT, and calibration of the wrinkle wavelength with the RIE time. This material is available free of charge via the Internet at http://pubs.acs.org.

AUTHOR INFORMATION

Corresponding Author

*E-mail: todom@northwestern.edu.

Notes

The authors declare no competing financial interest.

ACKNOWLEDGMENTS

This work was supported by the National Science Foundation (NSF) under NSF Award CMMI-1069180 and the Office of Naval Research (Grant N00014-13-1-0172). This research was conducted with Government support under Grants FA9550-05-C-0059 (to M.D.H.) and FA9550-11-C-0028 (to A.J.H.) and awarded by a Department of Defense, Air Force Office of Scientific Research, National Defense Science and Engineering Graduate Fellowship (32 CFR 168a). M.D.H. and C.J.E. gratefully acknowledge support from the Ryan Fellowship and the Northwestern University International Institute for Nanotechnology. C.J.E. and A.J.H. acknowledge a Hierarchical Materials Cluster Program (HMCP) Fellowship. HMCP is sponsored by The Graduate School at Northwestern University. This work made use of the NUANCE Center facilities, which are supported by NSF-MRSEC, NSF-NSC, the Keck Foundation, and the Materials Processing and Microfabrication Facility, which is supported by the MRSEC program of the NSF (Grant DMR-1121262).

REFERENCES

(1) Efimenko, K.; Rackaitis, M.; Manias, E.; Vaziri, A.; Mahadevan, L.; Genzer, J. *Nat. Mater.* **2005**, *4*, 293−297.
(2) Mei, Y.; Kiravittaya, S.; Harazim, S.; Schmidt, O. G. *Mater. Sci. Eng., R* **2010**, *70*, 209−224.
(3) Moon, M.; Lee, S.; Sun, J.; Oh, K.; Vaziri, A.; Hutchinson, J. *Proc. Natl. Acad. Sci. U.S.A.* **2007**, *104*, 1130−1133.
(4) Kim, J. B.; Kim, P.; Pegard, N. C.; Oh, S. J.; Kagan, C. R.; Fleischer, J. W.; Stone, H. A.; Loo, Y.-L. *Nat. Photonics* **2012**, *6*, 327−332.
(5) Bowden, N.; Brittain, S.; Evans, A.; Hutchinson, J.; Whitesides, G. *Nature* **1998**, *393*, 146−149.
(6) Kim, P.; Abkarian, M.; Stone, H. A. *Nat. Mater.* **2011**, *10*, 952−957.
(7) Fu, C.; Grimes, A.; Long, M.; Ferri, C.; Rich, B.; Ghosh, S.; Lee, L.; Gopinathan, A.; Khine, M. *Adv. Mater.* **2009**, *21*, 4472−4476.
(8) Genzer, J.; Groenewold, J. *Soft Matter* **2006**, *2*, 310−323.
(9) Lin, P.; Yang, S. *Appl. Phys. Lett.* **2007**, *90*, 241903.
(10) Stafford, C. M.; Harrison, C.; Beers, K. L.; Karim, A.; Amis, E. J.; Vanlandingham, M. R.; Kim, H.; Volksen, W.; Miller, R. D.; Simonyi, E. E. *Nat. Mater.* **2004**, *3*, 545−550.
(11) Qi, Y.; Jafferis, N. T.; Lyons, K.; Lee, C. M.; Ahmad, H.; McAlpine, M. C. *Nano Lett.* **2010**, *10*, 524−528.
(12) Sun, Y.; Choi, W. M.; Jiang, H.; Huang, Y. Y.; Rogers, J. A. *Nat. Nanotechnol.* **2006**, *1*, 201−207.
(13) Khang, D.-Y.; Jiang, H.; Huang, Y.; Rogers, J. A. *Science* **2006**, *311*, 208−212.
(14) Zhao, Y.; Huang, W. M.; Fu, Y. Q. *J. Micromech. Microeng.* **2011**, *21*, 067007.
(15) Zhao, X.; Xia, Y.; Schueller, O.; Qin, D.; Whitesides, G. *Sens. Actuators, A* **1998**, *65*, 209−217.
(16) Zang, J. F.; Zhao, X. H.; Cao, Y. P.; Hutchinson, J. W. *J. Mech. Phys. Solids* **2012**, *60*, 1265−1279.
(17) Ada, E. T.; Kornienko, O.; Hanley, L. *J. Phys. Chem. B* **1998**, *102*, 3959−3966.
(18) Verma, A.; Sharma, A.; Kulkarni, G. *Small* **2011**, *7*, 758−765.
(19) Lee, J.; Ro, H. W.; Huang, R.; Lemaillet, P.; Germer, T. A.; Soles, C. L.; Stafford, C. M. *Nano Lett.* **2012**, *12*, 5995−5999.
(20) Ouyang, M.; Yuan, C.; Muisener, R. J.; Boulares, A.; Koberstein, J. T. *Chem. Mater.* **2000**, *12*, 1591−1596.
(21) Yu, C.; Masarapu, C.; Rong, J.; Wei, B.; Jiang, H. *Adv. Mater.* **2009**, *21*, 4793−4797.
(22) Bonaccurso, E.; Graf, K. *Langmuir* **2004**, *20*, 11183−11190.
(23) Lock, E.; Petrovykh, D.; Mack, P.; Carney, T.; White, R.; Walton, S.; Fernsler, R. *Langmuir* **2010**, *26*, 8857−8868.
(24) Chan, C. M.; Ko, T. M.; Hiraoka, H. *Surf. Sci. Rep.* **1996**, *24*, 3−54.
(25) Huck, W. T. S.; Bowden, N.; Onck, P.; Pardoen, T.; Hutchinson, J. W.; Whitesides, G. M. *Langmuir* **2000**, *16*, 3497−3501.
(26) *Guide to Using Wvase32*; J. A. Woollam Co., Inc.
(27) Harland, G. Tomkins, E. A. I. *Handbook of Ellipsometry*, 1st ed.; William Andrew Publishing: New York, 2005; Vol. *1*, p 870.
(28) Hale, G. M.; Querry, M. R. *Appl. Opt.* **1973**, *12*, 555−563.